

Microstructure parameters and optical properties of cadmium ferrite thin films of variable thickness

E.R. Shaaban

Received: 28 September 2012 / Accepted: 25 July 2013 / Published online: 24 August 2013
© Springer-Verlag Berlin Heidelberg 2013

Abstract CdFe₂O₄ thin films of different thicknesses were deposited onto glass substrates by the thermal evaporation technique. Their structural characteristics were studied by X-ray diffraction (XRD). The microstructure parameters, crystallite size, and microstrain were calculated. It is observed that both the crystallite size increases and microstrain increase with increasing with the film thickness. The fundamental optical parameters like absorption coefficient and optical band gap are calculated in the strong absorption region of transmittance and reflectance spectrum. The refractive indices have been evaluated in terms of the envelope method, which has been suggested by Swanepoel in the transparent region. The refractive index can be extrapolated by the Cauchy dispersion relationship over the whole spectra range, which extended from 400 to 2500 nm. The refractive index, n , increases on increasing the film thickness up to 733 nm and the variation of n with higher thickness lies within the experimental errors.

1 Introduction

The gas sensor has recently attracted much attention due to increasing demand of environmental monitoring and other gas detecting applications. Among different types of gas sensor, the thin film gas sensor has been much of interest because of microelectronic batch-fabricated compatibility, reproducibility, and ability to form multilayer device structures. Dilute magnetic semiconductors (DMS) are a

highly topical area of interest due to the possibility of integrating them into new or existing electronic and optoelectronic devices in order to provide increased functionality by the provision of an additional electronic state. Cadmium ferrite (CdFe₂O₄) is an important complex oxide in gas-sensing materials. Several synthetic approaches have been used to prepare CdFe₂O₄ particles including the combustion method [1], co-precipitation [2, 3], ball milling [4, 5], sol gel [6], pulsed laser deposition (PLD) [7] and so on. Detailed studies on their structural [3, 4], and magnetic properties [2, 4] and [5] and electrical conductivity [7] have been investigated and reported. The magneto-optical properties of a highly stable ionic magnetic fluid sample containing CdFe₂O₄ nanoparticles also were investigated [8]. Hence, the present work has a twofold purpose: the first purpose is to study the effect of film thickness on both microstructure parameter (crystallite size and microstrain) and optical constants of CdFe₂O₄ thin films obtained by the vacuum evaporation technique. The second purpose is to interpret the behavior of the optical constants on the microstructure parameters of the films.

2 Experimental details

Polycrystalline sample of CdFe₂O₄ was prepared by the solid-state reaction method. Stoichiometric amounts of high-purity (99.999 %) analytical grade CdO and Fe₂O₃ powders (Sigma-Aldrich Co., USA) were mixed by grinding in a mortar for about 12 hours. The powders were pressed into a disk-shape pellet. Direct evaporation of the mixture in powder form resulted in sputtering of the powder when the boat is heated. Thin films of CdFe₂O₄ with various thicknesses were prepared by electron beam evaporation using high vacuum coating unit type Edward Auto

E.R. Shaaban (✉)
Department of Physics, Faculty of Science, Al-Azhar University,
Assiut, 71542, Egypt
e-mail: esam_ramadan2008@yahoo.com
Fax: +20-88-2365432

306. The system was pumped to a pressure of 5×10^{-6} Pa. The films were deposited on amorphous glass substrates (25 mm \times 25 mm) and maintained at room temperature (300 K). The substrates were carefully cleaned by using acetone and distilled water. The thickness of the films was kept to be constant at 720 nm (± 10 nm) for all composition studies. The substrates were rotated during the deposition. The source to the substrate distance was about 20 cm to get a deposition rate of 2 nm/sec. The thickness of the films and the rates of evaporation were monitored with a quartz crystal thickness monitor attached to the vacuum system. For more details about the applied methodology, see e.g. [9, 10]. The structure and phase purity of the samples and as-deposited films were checked at room temperature by means of X-ray powder diffraction (XRD) Shimadzu Diffractometer XRD 6000, Japan, with Cu-K α 1 radiation ($\lambda = 1.54056$ Å). The data were collected by step-scan modes in a θ - 2θ range between 10° and 70° with step-size of 0.02° and step time of 0.6 seconds. Pure silicon \sim Si 99.9999 % was used as an internal standard. The elemental composition of the films was analyzed by using energy dispersive X-ray spectrometer unit (EDXS) interfaced with a scanning electron microscope, SEM (JOEL XL) operating an accelerating voltage of 30 kV, which was used to study the morphology of the film. The relative error of determining the indicated elements does not exceed 2 %. Optical characterization of the films has been performed from spectral transmittance and reflectance, which were obtained through a JASCO V-670 double beam spectrophotometer. The measurements have been performed in the wavelength range from 400 to 2500 nm. The transmittance and reflectance measurements were taken at normal incident.

3 Results and discussion

3.1 Microstructure parameters

The XRD pattern of the CdFe₂O₄ films of different thicknesses is shown in Fig. 1. Only four diffraction peaks corresponding to the (311), (400), (422), and (511) reflections of CdFe₂O₄ are present according to (JCPDF card number 22-1063), which indicates that single spinel phase CdFe₂O₄ thin film was obtained. It can be seen that the film thickness affects the XRD pattern of CdFe₂O₄ thin films i.e. the peak intensity increases with increasing film thickness. Each X-ray diffraction line profile obtained in a diffractometer is broadened due to instrumental and physical factors (crystallite size and lattice strains) [11]. Therefore, the first indispensable step preparatory to the calculation of crystallite size and lattice strain from the recorded XRD scan is a determination of the “pure” diffraction line profile for a given reflection whose full-width at half maximum (FWHM) depends solely on the physical factors [11]. This “pure” line

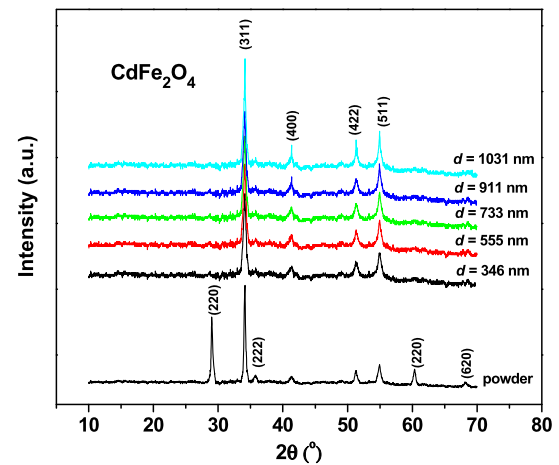


Fig. 1 The XRD patterns of films of different thicknesses on glass substrates and the reference powder of CdFe₂O₄

profile is extracted by removing (deconvoluting) the instrumental broadening factor from the experimental line profile. Only then the “pure” line profile can be used for calculating the crystallite size and lattice strain. Simple equations or graphs based on line profiles of assumed analytical forms can be used for the instrumental broadening correction [11]. In the present work, the instrumental broadening-corrected “pure” FWHM of each reflection was calculated from the parabolic approximation correction [11]:

$$\Delta 2\theta = B \left(1 - \frac{b^2}{B^2} \right) \text{ (rad)} \quad (1)$$

where B and b are the FWHM (in radians) of the same Bragg-peak from the XRD scans of the experimental and reference powder, respectively. The reference powder was the same powdered CdFe₂O₄ annealed at 400 °C for 2 h. The XRD pattern of the CdFe₂O₄ polycrystalline reference powder is shown in Fig. 1. All of the diffraction peaks can be indexed to the pure cubic CdFe₂O₄ (JCPDF card number 22-1063) and no other phases are present. From Fig. 1 the FWHM was found to decrease markedly with increasing film thickness. The method was based on the assumption that the crystallite size and strain line profiles are both presumed to be Cauchy and the appropriate equation for the separation of crystallite size and strain takes the following form [11]:

$$\Delta(2\theta) \cos \theta_0 = \frac{\lambda}{D_v} + 4e(\sin \theta_0) \quad (2)$$

Figure 2 shows the full width of the (311), (400), (422) and (511) reflections, scaled in terms of $\Delta(2\theta) \cos(\theta_0)$ vs. $\sin(\theta_0)$ are the Bragg angle and the FWHM [12–14]. The values of e and D_v can be calculated from the slope and the ordinate intersection, respectively. Equation (2) was first proposed by Williamson and Hall [15] and is customarily referred to as the “Williamson–Hall method” [16–18]. The

inset of Fig. 2 shows a comparative look of microstructure parameters of both crystallite size (D_v) and microstrain of the CdFe_2O_4 films of different thicknesses on glass substrates. It is observed that the crystallite size increases with increase the film thickness. The increasing in crystallite size with increasing the film thickness is in good agreement with previously reported results [14, 19]. The increase in crystallite size may attribute to the decrease in the FWHM at each reflection with increasing the film thickness and also may be interpreted in terms of a columnar grain growth. On the other hand the microstrain exhibited the same behavior i.e. increases with increasing the film thickness, such an increase in microstrain may be due to the decrease in lattice defects among the grain boundary. Thicker films are characterized by more homogeneous network, which minimizes the number of defects and localized states, and thus the microstrain increases [20].

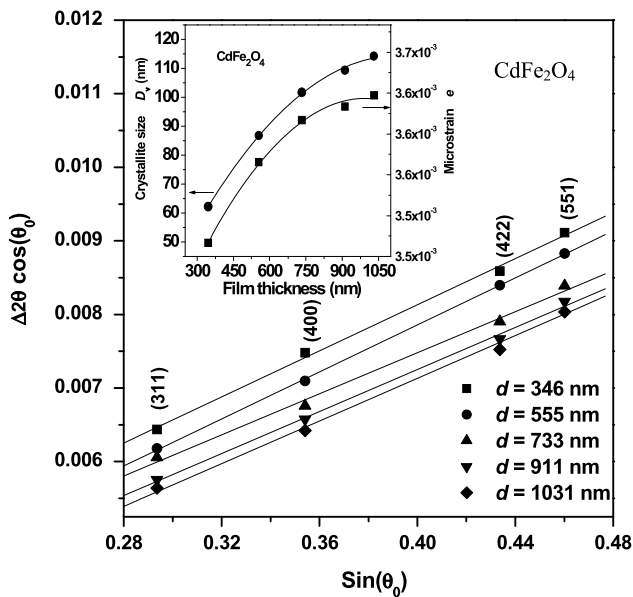
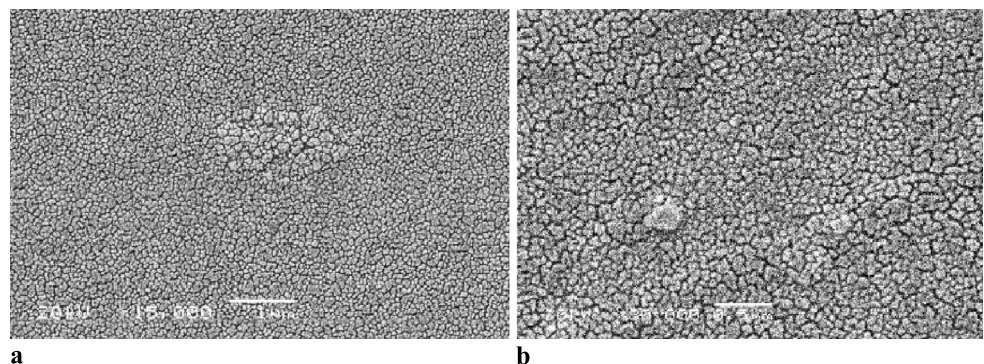


Fig. 2 Crystallite size/strain separation calculating using $\Delta 2\theta$ breadth according to “Williamson Hall” method and the inset shows the effect of film thickness on both crystallite size and microstrain of CdFe_2O_4 thin films

Fig. 3 Scanning electron microscope micrographs for (a) $d = 555$ nm and (b) $d = 1033$ nm of CdFe_2O_4 thin film



Furthermore, SEM measurements are carried out to determine the surface topology and morphology of the CdFe_2O_4 thin films at room temperature. Figures 3(a, b) shows typical SEM photographs for CdFe_2O_4 films at thickness 555 and 1033 nm, respectively. The films exhibit smooth fine grainy surface. The crystallite size evaluated from SEM image was found to be about 80 nm for $d = 555$ nm and about 108 nm $d = 1033$ nm, which agrees with the value calculated from XRD technique (86 nm for $d = 555$ nm and 114 nm for $d = 1033$).

3.2 Absorption coefficient and the optical band gap

The spectral dependence of the optical transmittance $T(\lambda)$ and reflectance $R(\lambda)$ of the investigated sample can be obtained using double beam spectrophotometer. The variation of absolute value of $T(\lambda)$ and $R(\lambda)$ against wavelength λ is shown in Fig. 4. In a wide spectral range (400–2500 nm), an experimental result showing the variation of reflection $R(\lambda)$ and transmission $T(\lambda)$ of a crystalline thin film of different thicknesses of CdFe_2O_4 thin films is presented in Fig. 4. As clearly observed in the transmission spectrum, distinct interference fringes are observed at longer wavelength (transparent region) with large intensity approaching 87 %. As we move to shorter wavelength where the absorption starts to take place within the film, the intensity of the interference fringes starts to decrease gradually until it approaches the strong absorption region at the edge of the optical band gap of the deposited films. The experimental results of the transmission $T(\lambda)$ show a clear shift from longer wavelength to shorter wavelength at increasing film thickness. Such shifts are a direct consequence of the thickness dependence of the optical band gap of the CdFe_2O_4 thin films.

The absorption coefficient α can be obtained from the experimentally measured values of R and T in the strong absorption region according to the following expression [21]:

$$\alpha = \frac{1}{d} \ln \left[\frac{(1 - R)^2 + [(1 - R)^4 + 4R^2T^2]^{1/2}}{2T} \right] \quad (3)$$

where d is the sample thickness.

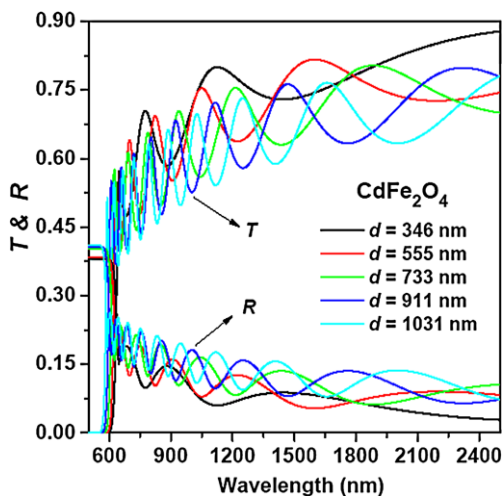


Fig. 4 Transmittance and reflectance spectrum for CdFe₂O₄ thin films with different thickness

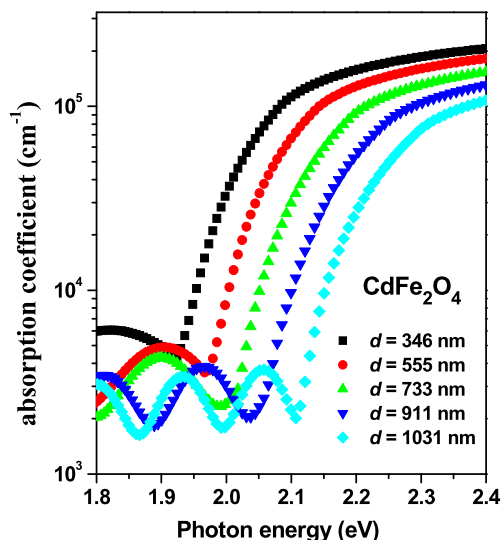


Fig. 5 Variation of absorption coefficient α versus $h\nu$ for CdFe₂O₄ films with different thickness

Figure 5 shows dependence of the absorption coefficient $\alpha(h\nu)$ on photon energy as a function of film thickness for CdFe₂O₄ thin films. The study of the optical absorption spectra in the CdFe₂O₄ is important since they provide essential information about the band structure and optical band gap. It is well known that the higher energy part of the optical absorption spectra gives information about the electronic states in the material, while the other lower energy part of the spectrum corresponds to atomic vibrations. Generally, the optical absorption spectra of CdFe₂O₄ have been found to have three distinct regions: the weak absorption region, which originate from defects and impurities; the absorption edge region, which is strongly related to the structural disorder of the system; and finally, the strong absorption region, which determines the optical band gap. It is clearly observed

that in the absorption edge region the absorption coefficients decrease with the increase of the film thickness. Figure 5 further shows that the absorption edge shifts toward the lower energy region with increasing the film thickness. It is known that pure CdFe₂O₄ compounds have a sharp absorption edge [22–27].

It is known that in the vicinity of the fundamental absorption edge, for allowed direct band-to-band transitions, the absorption coefficient is described by

$$\alpha(h\nu) = \frac{K(h\nu - E_g^{\text{opt}})^m}{h\nu} \quad (4)$$

where K is a characteristic parameter (independent of photon energy) for respective transitions [28], $h\nu$ denotes photon energy, E_g^{opt} is the optical energy gap and m is a number which characterizes the transition process. Different authors [29–31] have suggested different values of m for different glasses, $m = 2$ for most amorphous semiconductors (indirect transition) and $m = 1/2$ for most of crystalline semiconductor (direct transition). In the case of different thicknesses of polycrystalline of CdFe₂O₄ thin films the direct cases are valid. For higher values ($\alpha \geq 10^4 \text{ cm}^{-1}$) of the absorption coefficient α (where the absorption is associated with inter-band transitions), the energy gap can be determined. Figure 6 is a typical best fit of $(\alpha h\nu)^2$ vs. photon energy ($h\nu$) for different thicknesses of the CdFe₂O₄ thin films. The extrapolation at the linear part in the $(\alpha h\nu)^2$ vs. $(h\nu)$ at $(\alpha h\nu)^2 = 0$ (for the allowed direct transition) for different thicknesses of CdFe₂O₄ thin films is shown. The variation of direct band gap with the thickness is shown in the inset of Fig. 6. The values of E_g^{opt} for both direct transition is found to increase with increasing film thickness up to 733 nm and then the variation of E_g^{opt} with higher thickness lies within the experimental errors.

Accordingly, one can expect that the E_g^{opt} decreases with increasing the film thickness because crystal defects can be formed which produce localized states that change the effective Fermi level due to an increase in carrier concentrations [20]. But thicker films are characterized by a more homogeneous network, which minimizes the number of defects and localized states, and thus the optical band gap increases [32, 33]. The increase of E_g^{opt} for direct transition may be also attributed to the increase in crystallite size and microstrain. Cheng et al. and Sultan et al. have investigated the electronic structure of CdFe₂O₄ by DFT (density functional theory) method [34, 35]. Their results showed that the bandgap of CdFe₂O₄ was about 2.0 eV; this value is in agreement with our experimental result.

3.3 Refractive index and film thickness

The refractive index was determined using Swanepoel's method (method of recording envelopes around the interference maxima and minima of the transmittance spectra

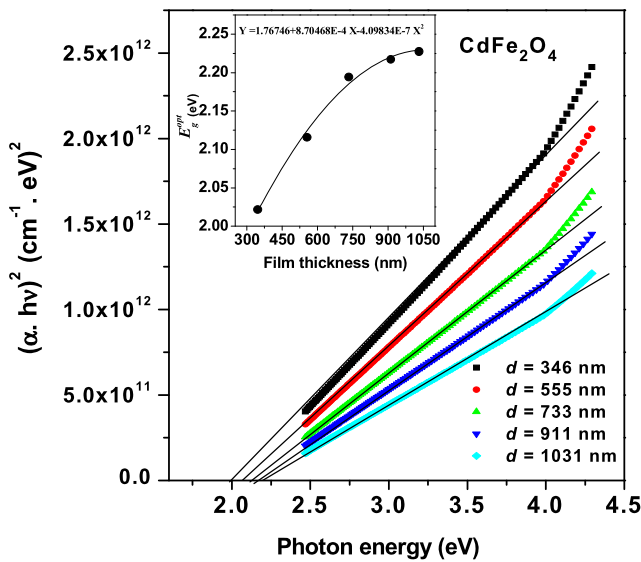


Fig. 6 Variation of $(\alpha \cdot hv)^2$ vs. (hv) for $CdFe_2O_4$ films with different thicknesses and the inset shows the effect of film thickness on the energy gap of $CdFe_2O_4$ thin films

[22, 23, 29]). Figures 7(a, b) illustrates the typical transmittance spectra for $d = 555$ nm and $d = 1031$ nm of $CdFe_2O_4$ thin films. As shown in Figs. 7(a, b), the observed number of interference fringes increases with increasing film thickness. According to this method, the value of the refractive index at a determined wavelength can be calculated using the expression [24, 25, 36, 37]

$$n = [N_1 + (N_1^2 - s^2)^{\frac{1}{2}}]^{\frac{1}{2}} \tag{5}$$

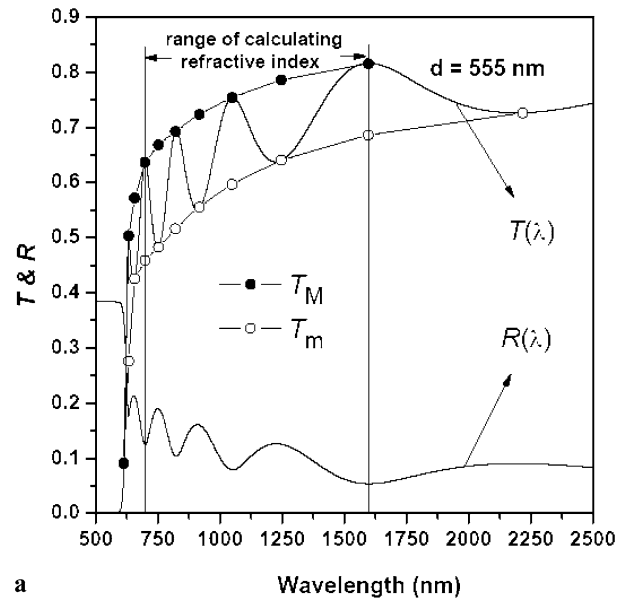
where

$$N_1 = 2s \frac{T_M - T_m}{T_M T_m} + \frac{s^2 + 1}{2}$$

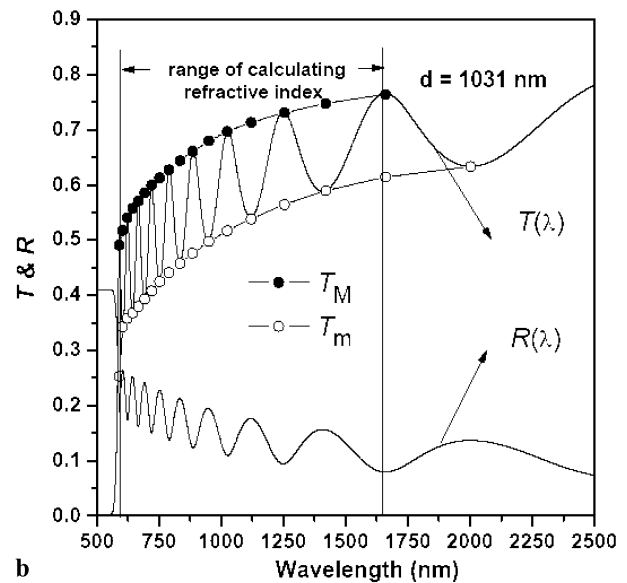
Here T_M and T_m , are the transmittance maximum and the corresponding minimum at a certain wavelength λ . Alternatively, one of these values is an experimental interference extreme and the other one is derived from the corresponding envelope; both envelopes were computer-generated using the program Origin version 7 (OriginLab Corp.) and drawn around the extrema of each transmittance spectrum (see Figs. 7(a, b)). On the other hand, the necessary values of the refractive index of the substrate are obtained from the transmittance spectrum of the substrate, T_s using the well-known equation

$$s = \frac{1}{T_s} + \left(\frac{1}{T_s} - 1 \right)^{\frac{1}{2}} \tag{6}$$

The values of the refractive index n , as calculated from Eq. (5) are shown in Fig. 8. Moreover, if n_{e1} and n_{e2} are the refractive indices at two adjacent maxima (or minima) at



a



b

Fig. 7 The typical transmittance spectra for (a) $d = 555$ nm and (b) $d = 1033$ nm of $CdFe_2O_4$ thin film. Curves T_M , and T_m , according to the text

λ_1 and λ_2 , it follows that the film thickness is given by the expression

$$d = \frac{\lambda_1 \lambda_2}{2(\lambda_1 n_{e2} - \lambda_2 n_{e1})} \tag{7}$$

The values of the film thicknesses of the $CdFe_2O_4$ thin films are 346, 555, 733, 911, 1031 nm. It is observed that, for all investigated films, the refractive index n decreases with increasing wavelength showing normal dispersion following the two-term Cauchy dispersion relationship, $n(\lambda) = a + b/\lambda^2$, which can be used for extrapolation of the whole wavelengths [38] as shown in Fig. 8. The least squares fit of the two sets of values of n for the different samples are

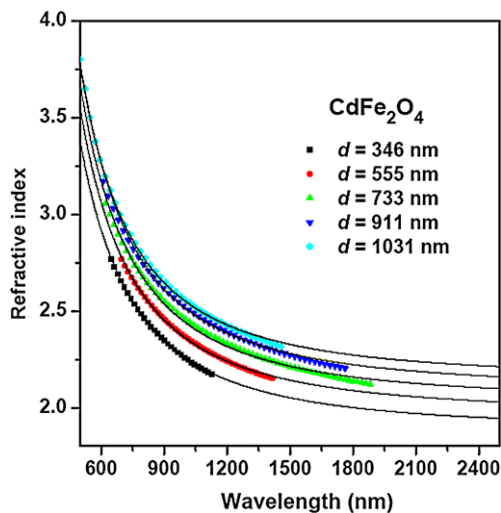


Fig. 8 The spectral dependence of refractive index n of CdFe_2O_4 films with different thicknesses

$n = 1.88 + 3.73 \times 10^5/\lambda^2$ for $d = 346$ nm, $n = 1.97 + 3.95 \times 10^5/\lambda^2$ for $d = 555$ nm, $n = 2.03 + 4.09 \times 10^5/\lambda^2$ for $d = 733$ nm, $n = 2.11 + 4.27 \times 10^5/\lambda^2$ for $d = 911$ nm and $n = 2.15 + 4.28 \times 10^4/\lambda^2$ for $d = 1031$ nm. Figure 8 illustrates the refractive index, n , versus λ for different thicknesses of the CdFe_2O_4 thin films. From this figure the refractive index decreases with increasing wavelength showing normal dispersion behavior. In addition, the magnitude of the refractive index increases notably with increasing the film thickness for different film thicknesses up to 733 nm and then the variation of n with higher thicknesses lies within the experimental errors. The increase in refractive index with increasing film thickness is in a good agreement with previously reported results [39, 40].

4 Conclusions

Polycrystalline CdFe_2O_4 films of different thicknesses have been deposited onto glass substrates at room temperature by the vacuum evaporation technique. From XRD studies it is found that the film is polycrystalline in nature and the CdFe_2O_4 crystallites have cubic structure. The microstructure parameters of the CdFe_2O_4 thin films such as crystallite size (D_v) and microstrain e were calculated. It is observed that the crystallites sizes increase with increasing the film thickness. The microstrain shows an increase as the film grows due to the decrease in lattice defects which was pronounced at small thicknesses. The optical characterization of thermally evaporated polycrystalline CdFe_2O_4 films of five different thicknesses was made using the transmittance and reflectance spectra at normal incidence. The absorption coefficient and optical band gap are calculated in the strong absorption region of transmittance and reflectance spectra.

The values of E_g^{opt} for direct transition are found to increase with increasing film thickness up to 733 nm and then the variation of E_g^{opt} with higher thicknesses lie within experimental errors. The increase of E_g^{opt} for direct transitions may be attributed to the increase in crystallite size and microstrain.

The envelope method suggested by Swanepoel has been applied to the films with a reasonable number of interference fringes. The optical method applied here makes it possible to determine the refractive index and average thickness of the films. The results indicate that the values of n gradually increase with increasing film thickness up to 733 nm and then the variation of n with higher thickness lies within the experimental errors.

Acknowledgements The author is grateful to Al-Azhar university Faculty of Science Physics department Assiut branch for financial support.

References

1. P.K. Nayak, *Mater. Chem. Phys.* **112**, 24 (2008)
2. D.S. Mathew, R.-S. Juang, *Chem. Eng. J.* **129**, 51 (2007)
3. X. Chu, C. Zheng, *Sens. Actuators B, Chem.* **96**, 504 (2003)
4. C.N. Chinnasamy, A. Narayanasamy, N. Ponpandian, R.J. Joseyphus, *Scr. Mater.* **44**, 1411 (2001)
5. M.H. Mahmoud, A.M. Abdallas, H.H. Hamdeh, W.M. Hikal, S.M. Taher, J.C. Ho, *J. Magn. Magn. Mater.* **263**, 269 (2003)
6. X. Lou, S. Liu, D. Shi, W. Chu, *Mater. Chem. Phys.* **105**, 67 (2007)
7. F. Miao, Z. Deng, X. Lv, G. Gu, S. Wan, X. Fang, Q. Zhang, S. Yin, *Solid State Commun.* **150**, 2036 (2010)
8. A.F. Bakuzis, K. Skeff Neto, P.P. Gravina, L.C. Figueiredo, P.C. Morais, L.P. Silva, R.B. Azevedo, O. Silva, *Appl. Phys. Lett.* **84**, 2355 (2004)
9. M. El-Hagary, M. Emam-Ismael, E.R. Shaaban, A. Al-Rashidi, S. Althoyaib, *Mater. Chem. Phys.* **132**, 581 (2012)
10. E.R. Shaaban, I. Kansal, J.M.F. Ferreira, *Physica B, Condens. Matter* **404**, 3571 (2009)
11. H.P. Klug, L. Alexander, *X-Ray Diffraction Procedures for Polycrystalline and Amorphous Materials*, 2nd edn. (Wiley, New York, 1974), pp. 618–708, Chap. 9
12. H. Saryanto, S. Khaerudini Deni, P. Untoro, M.H. Saleh, D. Sebayang, *Adv. Mater. Res.* **129–131**, 999 (2010)
13. Z.R. Khan, M. Zulfeqar, M.S. Khan, *Bull. Mater. Sci.* **35**, 169 (2012)
14. E.R. Shaaban, N. Afify, A. El-Taher, *J. Alloys Compd.* **482**, 400 (2009)
15. G.K. Williamson, W.H. Hall, *Acta Metall.* **1**, 22–31 (1953)
16. D.G. Morris, M.A. Morris, M. LeBoeuf, *Mater. Sci. Eng.* **156**, 11 (1992)
17. G.H. Chen, C. Suryanarayana, F.H. Froes, *Metall. Mater. Trans. A, Phys. Metall. Mater. Sci.* **26**, 1379 (1995)
18. F.W. Gayle, F.S. Biancianiello, *Nanostruct. Mater.* **6**, 429 (1995)
19. F. Miao, Z. Deng, X. Lv, G. Gu, S. Wan, X. Fang, Q. Zhang, S. Yin, *Solid State Commun.* **150**, 2036 (2010)
20. S.K. Biswas, S. Chaudhuri, A. Choudhury, *Phys. Status Solidi A, Appl. Res.* **105**, 467 (1988)
21. E. Szewczak, J. Paszula, A.V. Leonov, H. Matyja, *Mater. Sci. Eng.* **226–228**, 115 (1997)
22. M. Kastner, *Phys. Rev. Lett.* **28**, 355 (1972)

23. L.L. Kazmersky (ed.), *Polycrystalline and Amorphous Thin Films and Devices* (Academic Press, New York, 1980), p. 135
24. R. Swanepoel, *J. Phys. E, Sci. Instrum.* **16**, 121 (1983)
25. R. Swanepoel, *J. Phys. E, Sci. Instrum.* **17**, 896 (1984)
26. E.R. Shaaban, M.F. Kaid, E. Moustafa, A. Adel, *J. Phys. D, Appl. Phys.* **41**, 53125301 (2008)
27. C. Baban, G.I. Rusu, *Appl. Surf. Sci.* **211**, 6 (2003)
28. M. Nowak, *Thin Solid Films* **266**, 258 (1995)
29. J.I. Pankove, *Optical Processes in Semiconductors* (Dover, New York, 1971), p. 44
30. E.A. Davis, N.F. Mott, *Philos. Mag.* **22**, 903 (1970)
31. E.R. Shaaban, M. Abdel-Rahman, Y. El Sayed, M.T. Dessouky, *Thin Solid Films* **515**, 3810 (2007)
32. K.I. Arshak, C. Ahogarth, *Thin Solid Films* **137**, 281 (1986)
33. B.A. Mansour, H. Shaban, S.A. Gad, Y.A. El-Gendy, A.M. Salem, *J. Ovonic Res.* **6**, 13 (2010)
34. C. Cheng, C.S. Liu, *J. Phys. Conf. Ser.* **145**, 012028 (2009)
35. M. Sultan, R. Singh, *J. Phys. D, Appl. Phys.* **42**, 115306 (2009)
36. E. Márquez, J.M. González-Leal, A.M. Bernal-Oliva, R. Jiménez-Garay, T. Wagner, *J. Non-Cryst. Solids* **354**, 503 (2008)
37. E.R. Shaaban, *Philos. Mag.* **88**, 781 (2008)
38. T.S. Moss, *Optical Properties of Semiconductors* (Butterworths, London, 1959)
39. E.R. Shaaban, *Mater. Chem. Phys.* **100**, 411 (2006)
40. N. Revathi, P. Prathap, K.T. Ramakrishna Reddy, *Solid State Sci.* **11**, 1288 (2009)